Contrastive Explanations for Reinforcement Learning via Embedded Self Predictions

Zhengxian Lin [1] Kim-Ho Lam [1] Alan Fern [1]

Abstract

We investigate a deep reinforcement learning (RL) architecture that supports explaining why a learned agent prefers one action over another. The key idea is to learn action-values that are directly represented via human-understandable properties of expected futures. This is realized via the embedded self-prediction (ESP) model, which learns said properties in terms of human provided features. Action preferences can then be explained by contrasting the future properties predicted for each action. To address cases where there are a large number of features, we develop a novel method for computing minimal sufficient explanations from an ESP. Our case studies in three domains, including a complex strategy game, show that ESP models can be effectively learned and support insightful explanations.

1. Introduction

Typically, an RL agent can only explain why it prefers action A over B by revealing the predicted values, which provide little insight into the preference. Rather, a human might explain the same preference by explicitly contrasting meaningful properties of the predicted futures following each action. In this work, we develop a model that allows RL agents to also explain action preferences by contrasting human-understandable future predictions. Our approach learns generalized value functions (GVFs) (13) to make the future predictions, which are able to predict the future accumulation of arbitrary features when following a policy. Thus, given human-understandable features, the corresponding GVFs capture meaningful properties of a policy's future trajectories. In this work, we assume that a sufficient and meaningful set of such features are provided.

[1]Department of EECS, University of Oregon State, Oregon, USA. Correspondence to: Zhengxian Lin <linzhe@oregonstate.edu>, Kim-Ho Lam <lamki@oregonstate.edu>, Alan Fern <Alan.Fern@oregonstate.edu>.

Proceedings of the 37^{th} International Conference on Machine Learning, Vienna, Austria, PMLR 119, 2020.

To support sound explanation of action preferences via GVFs, it is important that the agent uses the GVFs to form preferences. To achieve this, our first contribution is the *embedded self-prediction (ESP) model* (Section 2), where the key idea is to directly "embedded" meaningful GVFs in the agent's action-value function that are trained to be "self-predicting" of the agent's greedy policy based on that function. This opens the door to both meaningful and sound contrastive explanations in terms of GVFs. However, this circularly defined ESP model, i.e. the policy depends on the GVFs and the GVFs depend on the policy behavior, raise the question of whether it can be effectively trained in non-trivial domains. Our second contribution is the ESP-DQN learning algorithm (Section 3), which adapts DQN (8) to train ESP agents. We provide theoretical conditions for convergence in the table-based setting and show empirically that the algorithm is effective in challenging domains.

Because ESP models can combine the embedded GVFs non-linearly, it is not straightforward to compare the contributions of GVFs to action preferences for contrastive explanations. Our third contribution develops a novel application of the integrated gradient (IG) (12), which supports producing contrastive explanations that are sound in a well-defined sense (Section 4). In addition, to support cases with large numbers of features, we also use the notion of minimal-sufficient explanation, which can significantly simplify explanations while remaining sound. Our fourth contribution presents case studies in two RL benchmark environments and a complex real-time strategy game (Section 6), which demonstrate our explanations can provide significant insights into learned policies.

2. Embedded Self-Prediction Model

An MDP is a tuple $\langle S, A, T, R\rangle$, with states S, actions A, transition function $T(s, a, s')$, and reward function $R(s, a)$. A policy π maps states to actions and has Q-function $Q^{\pi}(s, a)$ giving the expected infinite-horizon β-discounted reward of following π after taking action a in s. The optimal policy π^* and Q-function Q^* satisfy $\pi^*(s) = \arg\max_a Q^*(s, a)$. Q^* can be computed given the MDP by repeated application of the *Bellman Backup Operator*, which for any Q-function Q, returns a new Q-function $B[Q](s, a) = R(s, a) + \beta \sum_{s'} T(s, a, s') \max_{a'} Q(s', a')$.

We focus on RL agents that learn an approximation $\hat{Q}$ of Q^* and follow the corresponding greedy policy $\hat{\pi}(s)$. We aim to explain a preference for action a over b in a state s; i.e. explain why $\hat{Q}(s,a) > \hat{Q}(s,b)$. Importantly, the explanations should be meaningful to humans and soundly reflect the actual agent preferences. Below, we define the embedded self-prediction model, which facilitates such explanations (Section 4) in terms of generalized value functions.

Generalized Value Functions (GVFs). GVFs (13) are a generalization of traditional value functions that accumulate arbitrary feature functions rather than reward functions. Specifically, given a policy π, an n-dimensional state-action feature function $F(s,a) = \langle f_1(s,a), \ldots, f_n(s,a)\rangle$, and a discount factor γ, the corresponding n-dimensional GVF, denoted $Q_F^\pi(s,a)$, is the expected infinite-horizon γ-discounted accumulation of F when following π after taking a in s. Given an MDP, policy π, and features function F, the GVF can be computed by iterating the *Bellman GVF operator*, which takes a GVF Q_F and returns a new GVF $B_F^\pi[Q_F](s,a) = F(s,a) + \gamma \sum_{s'} T(s,a,s') Q_F(s', \pi(s'))$.

To produce human-understandable explanations, we assume semantically-meaningful features are available, so that the corresponding GVFs describe meaningful properties of the expected future—e.g., expected energy usage, or time spent in a particular spatial region, or future change in altitude.

ESP Model Definition. Given policy π and features F, we can contrast actions a and b via the GVF difference $\Delta_F^\pi(s,a,b) = Q_F^\pi(s,a) - Q_F^\pi(s,b)$, which may highlight meaningful differences in how the actions impact the future. However, such differences, cannot necessarily be used to soundly explain an agent's preferences because the agent may not consider those GVFs. Thus, the ESP model forces agents to directly define action values, and hence preferences, in terms of GVFs of their own policies allowing for such differences to be used soundly.

The ESP model embeds a GVF of the agent's greedy policy $Q_F^{\hat{\pi}}$ into the agents Q-function $\hat{Q}$, via $\hat{Q}(s,a) = \hat{C}(\hat{Q}_F(s,a))$, where $\hat{C} : R^n \to R$ is a learned combining function from GVF vectors to action values. When the GVF discount factor γ is zero, the ESP model becomes a direct combination of the features, i.e. $\hat{Q}(s,a) = \hat{C}(F(s,a))$, which is the traditional approach to using features for function approximation. By using $\gamma > 0$ we can leverage human-provided features in a potentially more powerful way. Because an ESP agent represents action-values via GVF components, it is possible to produce sound contrastive explanations in terms of GVFs, as described in Section 4.

3. ESP Model Training: ESP-DQN

We represent the learned combining function, $\hat{C}$, and GVF, $\hat{Q}_F$, as DNNs with parameters θ_C and θ_F. The goal is to optimize the parameters so that $\hat{Q}(s,a) = \hat{C}(\hat{Q}_F(s,a))$ approximates Q^* and $\hat{Q}_F(s,a)$ approximates $Q_F^{\pi^*}(s,a)$. The GVF accuracy condition is important since humans will interpret the GVF values in explanations. A potential learning complication is the circular dependence where $Q_F^{\hat{\pi}}$ is both an input to $\hat{Q}$ and depends on $\hat{Q}$ through $\hat{\pi}$. Below we overview our learning algorithm, *ESP-DQN*, a variant of DQN (8). Complete pseudo-code is in the supplementary material.

ESP-DQN follows an ϵ-greedy exploration policy while adding transitions to a replay buffer $D = \{(s_i, a_i, r_i, F_i, s'_i)\}$, where F_i is the feature vector for GVF training. Each learning step updates θ_C and θ_F using a random mini-batch. Like DQN, updates are based on a *target network*, which uses a second set of *target parameters* θ'_C and θ'_F, defining target combining and GVF functions $\hat{C}'$ and $\hat{Q}'_F$, yield target Q-function $\hat{Q}'(s,a) = \hat{C}'(\hat{Q}'_F(s,a))$. The target parameters are updated to the values of the non-target parameters every K learning steps and otherwise held fixed.

Combination Function Update. Since the output of $\hat{C}$ should approximate Q^*, optimizing θ_C can use traditional DQN updates. The updates, however, only impact θ_C while keeping θ_F fixed so that the GVF output $\hat{Q}_F(s,a)$ is viewed as a fixed input to $\hat{C}$. Given a mini-batch the update to θ_C is based on L2 loss with a target value for sample i being $y_i = r_i + \beta \hat{Q}'(s'_i, \hat{a}'_i)$, where $\hat{a}'_i = \arg\max_a \hat{Q}'(s', a)$ is the greedy action of the target network.

GVF Update. Training Q_F^π is similar to learning a critic in actor-critic methods for the evolving greedy policy, but instead of learning to predict long-term reward, we predict the long-term accumulation of F. Given a mini-batch we update θ_F based on L2 loss at the output of $\hat{Q}_F$ with respect to a target value $y_i = F_i + \gamma \hat{Q}'_F(s'_i, \hat{a}'_i)$, where $\hat{a}_i$ is the same target greedy action from above.

Convergence. Most combinations of function approximation and Q-learning, including DQN, do not have general convergence guarantees (14). Rather, for table-based representations that record a value for each state-action pair, Q-learning, from which DQN is derived, almost surely converges to Q^* (18), which at least shows that DQN is built on sound principles. We now consider convergence for ESP-Table, a table-based analog of ESP-DQN.

ESP-Table uses size 1 mini-batches and updates target tables (i.e. analogs of target networks) every K steps. The $\hat{Q}_F$ table is over state-action pairs, while for $\hat{C}$ we assume a hash function h that maps its continuous GVF inputs to a finite table. For example, since GVFs are bounded, this can be done with arbitrarily small error via quantization. A pair of feature and hash function (F, h) must be sufficiently expressive to provide any convergence guarantee. First, we assume h is *locally consistent*, meaning that for any input q there exists a finite ϵ such that for all $|q' - q| \leq \epsilon$, $h(q) = h(q')$. Second, we assume the pair (F, h) is *Bellman Sufficient*, which characterizes the representational capacity of the $\hat{C}$ table after Bellman GVF backups (see Section 2) with respect to representing Bellman backups.

Definition 1 (Bellman Sufficiency). *Feature-hash pair (F, h) is* Bellman sufficient *if for any ESP model $\hat{Q}(s,a) = \hat{C}(\hat{Q}_F(s,a))$ with greedy policy $\hat{\pi}$ and state-action pairs (s,a) and (x,y), if $h(\hat{Q}^+_F(s,a)) = h(\hat{Q}^+_F(x,y))$ then $B[\hat{Q}](s,a) = B[\hat{Q}](x,y)$, where $\hat{Q}^+_F = B^{\hat{\pi}}_F[\hat{Q}_F]$.*

Let $\hat{C}^t$, $\hat{Q}^t_F$, $\hat{Q}^t$, and $\hat{\pi}^t$ be random variables denoting the learned combining function, GVF, corresponding Q-function, and greedy policy after t updates. The following gives conditions for convergence of $\hat{\pi}^t$ to π^* and $\hat{Q}^t_F$ to a neighborhood of Q^*_F given a large enough K. The proof is in the supplementary material. An open problem is whether a stronger convergence result holds for $K = 1$.

Theorem 1. *If ESP-Table is run under the conditions for the almost surely (a.s.) convergence of Q-learning*[1] *and uses a Bellman-sufficient pair (F, h) with locally consistent h, then for any $\epsilon > 0$ there exists a finite target update interval K, such that for all s and a, $\hat{\pi}^t(s)$ converges a.s. to $\pi^*(s)$ and $\lim_{t\to\infty} |\hat{Q}^t_F(s,a) - Q^*(s,a)| \leq \epsilon$ with probability 1.*

4. ESP Contrastive Explanations

We focus on contrastive explanation of a preference, $\hat{Q}(s,a) > \hat{Q}(s,b)$, that decompose the preference magnitude $\hat{Q}(s,a) - \hat{Q}(s,b)$ in terms of components of the GVF difference vector $\Delta_F(s,a,b) = \hat{Q}_F(s,a) - \hat{Q}_F(s,b)$. Explanations will be tuples $\langle \Delta_F(s,a,b), W(s,a,b)\rangle$, where $W(s,a,b) \in R^n$ is an attribution weight vector corresponding to $\Delta_F(s,a,b)$. The meaningfulness of an explanation is largely determined by the meaningfulness of the GVF features. We say that an explanation is sound if $\hat{Q}(s,a) - \hat{Q}(s,a) = W(s,a,b) \cdot \Delta_F(s,a,b)$, i.e. it accounts for the preference magnitude. We are interested in explanation methods that only return sound explanations, since these explanations can be viewed as certificates for the agent's preferences. In particular, the definition implies that $W(s,a,b) \cdot \Delta_F(s,a,b) > 0$ if and only if $\hat{Q}(s,a) > \hat{Q}(s,b)$. In the simple case of a linear combining function $\hat{C}$ with weights $w \in R^n$, the preference magnitude factors as $\hat{Q}(s,a) - \hat{Q}(s,b) = w \cdot \Delta_F(s,a,b)$. Thus, $\langle \Delta_F(s,a,b), w\rangle$ is a sound explanation for any preference.

Non-Linear Combining Functions. Since the above linear factoring does not directly hold for non-linear $\hat{C}$, we draw on the *Integrated Gradient (IG)* (12), which was originally developed to score feature importance of a single input relative to a "baseline" input. We adapt IG to our setting by treating the less preferred action as the baseline, which we describe below in the terminology of this paper.

Let $X_{sa} = \hat{Q}_F(s,a)$ and $X_{sb} = \hat{Q}_F(s,b)$ be the GVF outputs of the compared actions. Given a differentiable combining function $\hat{C}$, IG computes an attribution weight $\theta_i(s,a,b)$ for component i by integrating the gradient of $\hat{C}$ while interpolating between X_a and X_b. That is, $\theta_i(s,a,b) = \int_0^1 \frac{\partial \hat{C}(X_{sb} + \alpha\cdot(X_{sa} - X_{sb}))}{\partial X_{sa,i}} \mathrm{d}\alpha$, which we approximate via finite differences. The key property is that the IG weights linearly attributes feature differences to the overall output difference, i.e. $\hat{C}(X_{sa}) - \hat{C}(X_{sb}) = \theta(s,a,b)\cdot(X_{sa} - X_{sb})$. Rewriting this gives the key relationship for the ESP model.

$$\hat{Q}(s,a) - \hat{Q}(s,b) = \theta(s,a,b) \cdot \Delta_F(s,a,b) \tag{1}$$

Thus, $\text{IGX}(s,a,b) = \langle \Delta_F(s,a,b), \theta(s,a,b)\rangle$ is a sound explanation, which generalizes the above linear case, since for linear $\hat{C}$ with weights w, we have $\theta(s,a,b) = w$. In practice, we typically visualize $\text{IGX}(s,a,b)$ by showing a bar for each component with magnitude $\theta_i(s,a,b) \cdot \Delta_F(s,a,b)$, reflecting the positive/negative preference contributions.

Minimal Sufficient Explanations. When there are many features $\text{IGX}(s,a,b)$ will likely overwhelm users. To soundly reduce the size, we use the concept of minimal sufficient explanation (MSX), which was recently developed for the more restricted space of linear reward-decomposition models (5). Equation 1, however, allows us to adapt the MSX to our non-linear setting. Let P and N be the indices of the GVF components that have positive and negative attribution to the preference, i.e., $P = \{i \ : \ \Delta_{F,i}(s,a,b) \cdot \theta_i(s,a,b) > 0\}$ and $N = \{1,\ldots,n\} - P$. For an arbitrary subset of indices E, let $S(E) = \sum_{i\in E} |\Delta_{F,i}(s,a,b) \cdot \theta_i(s,a,b)|$ be the total magnitude of the components, which lets the preference be expressed as $S(P) > S(N)$. Often only a small subset of positive components are required to overcome the negative components and maintain the preference. An MSX is simply a minimal set of such positive components. Thus, an MSX is given by $\arg\min\{|E| \ : \ E \subseteq P, S(E) > S(N)\}$, which is not unique in general. We select a solution that has the largest positive weight by sorting P and including indices into the MSX from largest to smallest.

5. Related Work

Linear reward-decomposition models with known weights have been studied for speeding up RL (15), multi-agent RL (10; 7), and explanation (5). These are special cases of the ESP model with known linear combining function. Generalized value function networks (11) are a related, but orthogonal, model that allows GVFs to accumulate other GVFs. Rather, we use GVFs as input to a combining network, which defines the GVF policy. Integrating GVF networks and ESP is an interesting direction.

[1]Specifically, each there must be an unbounded number of updates for each state-action pair and the learning rate schedule α_t must satisfy $\sum_t \alpha_t = \infty$ and $\sum_t \alpha_t^2 < \infty$.

The MSX for linear models was introduced for MDP planning (6) and then linear reward decomposition (5). We extend to the non-linear case. A recent approach to contrastive explanations (17) extracts properties from simulations of a policy at explanation time (17), which can be expensive. The explanations are not sound, since they are not tied to the agent's internal preference computation. Saliency explanation methods have been used in RL to highlight the important parts of the input (2; 4; 3; 1; 9). The explanations lack a clear semantics and hence any notion of soundness.

6. Experimental Case Studies

Below we introduce the three domains and features used for ESP agents and then overview our experiments, which aim to address the following questions: (1) (Section 6.2) Can we learn ESP models that perform as well as standard models? (2) (Section 6.2) Do the learned ESP models have accurate GVFs for the agent policy? (3) (Section 6.3) Do our explanations provide meaningful insight into agent preferences?

6.1. Environment Description

Lunar Lander and Cart Pole. We use the standard OpenAI Gym versions of Lunar Lander and Cart Pole. For Lunar Lander we defined 8 GVF features corresponding to the features used to compute its "shaping reward", e.g. distance to goal, velocity, etc. For Cart Pole we used 8 GVF features that discretized the numeric state into meaningful regions corresponding to an intuitive notion of safety. This includes two indicators for each of cart position, cart velocity, pole angle, and angle velocity. A perfectly balanced pole will always remain in the defined safe regions.

Tug of War. Tug of War (ToW) is a two-player zero-sum strategy game we designed using Blizzard's PySC2 interface to Starcraft 2. Our ToW domain is rich enough to be interesting for humans and presents many challenges to RL including an enormous state space, thousands of potential actions, long horizons, and sparse reward (win/loss).

ToW is played on a map divided into top and bottom horizontal lanes. Each lane has two bases structures at opposite ends, one for each player. The first player to destroy one of the opponent's bases in either lane wins. The game proceeds in 30 second waves. By the beginning of each wave, players must decide on either the top or bottom lane, and how many of each type of military production building to purchase for that lane. Purchases are constrained by the player's available currency, which is given at a fixed amount each wave. Each purchased building produces one unit of the specified type at the beginning of each wave. The units move across the lanes toward the opponent, engage enemy units, and attack the enemy base if close enough. The three types of units are Marines, Immortals, and Banelings, which have a rock-paper-scissors relationship and have different costs. If no base is destroyed after 40 waves, the player with the lowest base health loses. We trained a single agent against a reasonably strong agent produced via pool-based self-play learning (similar to AlphaStar training (16)).

We present two ToW ESP agents that use 17 and 131 structured GVF features. These feature sets are detailed in the supplementary material. The 17 features are organized into 3 groups: 1) Delta damage to each of the four bases by each of the three types of units; allowing GVFs to predict the amount of base damage done by each type of unit, giving insight into the strategy. 2) Indicators at the end of the game which specify which base had the lowest health. 3) An indicator of whether the game reaches 40 waves. (2) and (3) provide insight into the probability of each type of win/loss condition. The 131 features extend these to keep track of damage done in each lane to and from each combination of unit types along with additional information about the economy.

6.2. Learning Performance

To evaluate ESP learning compared to "standard" models we compare against two DQN instances: *DQN-full* uses the same overall network architecture as ESP-DQN, i.e. the GVF network structure feeding into the combining network. However, unlike ESP-DQN, DQN-full does not have access to GVF features and does not train the GVF network explicitly. It is possible DQN-full will suffer due to the bottleneck introduced at the GVF-combiner interface. Thus, we also evaluate DQN-combiner, which only uses the combining network of ESP-DQN, but directly connects that network to the raw agent input. Details of network architectures, optimizers, and hyperparameters are in the supplementary material.

Figure 1 (top row) shows the learning curves for the different agents and a random policy. Curves are averaged over 10 full training runs. For the control problems, CartPole and LunarLander, we see that all of the agents are statistically indistinguishable near the end of learning and reach peak performance after about the same amount of experience. This indicates that the potential complications of training the ESP model did not significantly impact performance in these domains. For ToW the ESP-DQN agents perform as well or better than the DQN variants. ESP-DQN with 17 features consistently converges to a win rate of nearly 100% and is more stable than the 131-feature version and other DQN variants. Interestingly, DQN-full with 17 features consistently fails to learn, which we hypothesize is due to the extreme 17 feature bottleneck inserted into the architecture. This is supported by seeing that with 131 features DQN-full does learn, though more slowly than ESP-DQN.

To evaluate the GVF accuracy of ESP-DQN we produce ground truth GVF data along the learning curves. Specifically, given the ESP policy $\hat{\pi}$ at any point, we use Monte-Carlo simulation to estimate $Q_F^{\hat{\pi}}(s, a)$ for all actions at a test set of states generated by running $\hat{\pi}$. Figure 1 (bottom row) shows the mean squared GVF prediction error on the test sets during learning. For each domain the GVF error is small at the end of learning and tends to rapidly decrease when the policy approaches its peak reward performance. LunarLander and ToW show a decrease of GVF error as learning progresses. CartPole, rather shows a sharp initial increase then sharp decrease. This is due to the initially bad policy always failing quickly, which trivializes GVF prediction. As the policy improves the GVFs become more challenging to predict leading to the initial error increase.

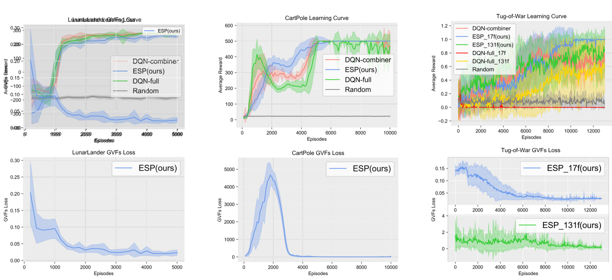

(a) Lunar Lander (b) Cart Pole (c) Tug-of-war

Figure 1: Reward learning curves (top) and GVF Loss curves (bottom) for the different agents in 3 environments.

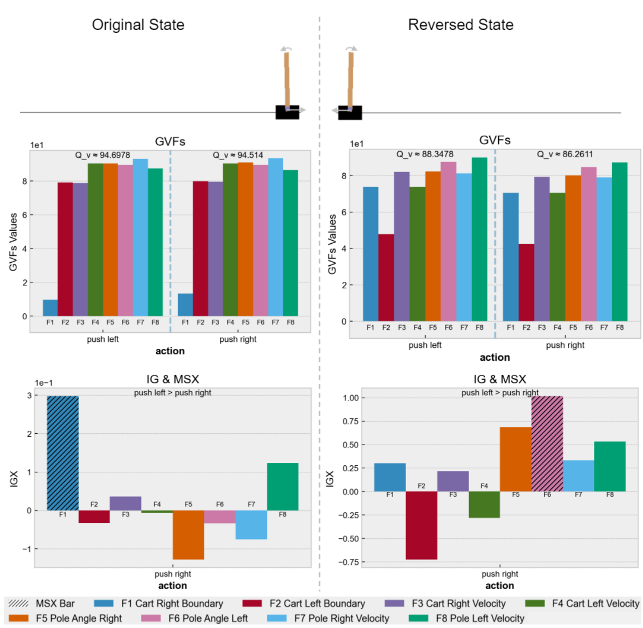

Figure 2: Examples of mirror states for CartPole. Each column gives the (top to bottom) game state; Q-value and GVFs; IGX and MSX. The bottom legend gives names of GVF features.

6.3. Example Explanations

Here we illustrate the contrastive explanations from our models. Due to space constraints the supplementary material includes a larger set of examples with detailed analysis in each domain.

Cart Pole. We compare a Cart Pole state-action explanation to an explanation produced by its reversed state as shown in Figure 2. This comparison illustrates how in one case, the explanation agrees with intuition and builds confidence in the policy; while the second case exposes an underlying inaccuracy or flaw.

Our original game state (left) positions the cart in a dangerous position moving right, close to the end of the track. The pole is almost vertical and has a small angle velocity towards the left. The action "push left" (move cart left) agrees with intuition as the cart is at the right edge of the screen and cannot move right without failing the scenario. The IG and MSX (left) concurs, showing the cart's current position close to the right edge as the main reason why it prefers the "push left" action over the "push right"; moving left will put the cart back within a safe boundary.

Reversing the game state (left) by multiplying -1 to each value in the input state vector produces a flipped game state (right). The cart is now positioned in a dangerous position moving left, close to the end of the track. Once again the pole is almost vertical and now has a small angle velocity towards the right. One would expect the agent to perform the action "push right" (the opposite action to game state (left)) as moving left will cause the agent to move off the screen and fail the scenario. However, as depicted in IG and MSX (right) we see the agent prefers "push left" over "push right". The agent justifies this action via an MSX that focuses on maintaining pole vertically to the left. This justification indicates that the agent is putting too much weight on the pole angle versus the boundary condition in this dangerous situation. The agent has not learned the critical importance of the left boundary. This indicates further training on the left side of the game map is needed. Presumably, during training the agent did not experience similar situations very often.

Tug of War. We give 2 examples from a high-performing 17 feature ESP agent, one that agrees with common sense and one that reveals a flaw. Additional examples for the 17 and 131 feature agents are in the supplementary material. Game state (top) illustrates that the ESP agent (blue player) has too few marine buildings to defend against the opponent's Immortals. We show information for the best ranked action and a sub-optimal action of interest (action details in caption). The best action creates units in the top lane, while the sub-optimal action creates the maximum possible units in the bottom lane. The IGX and MSX show (top) that the

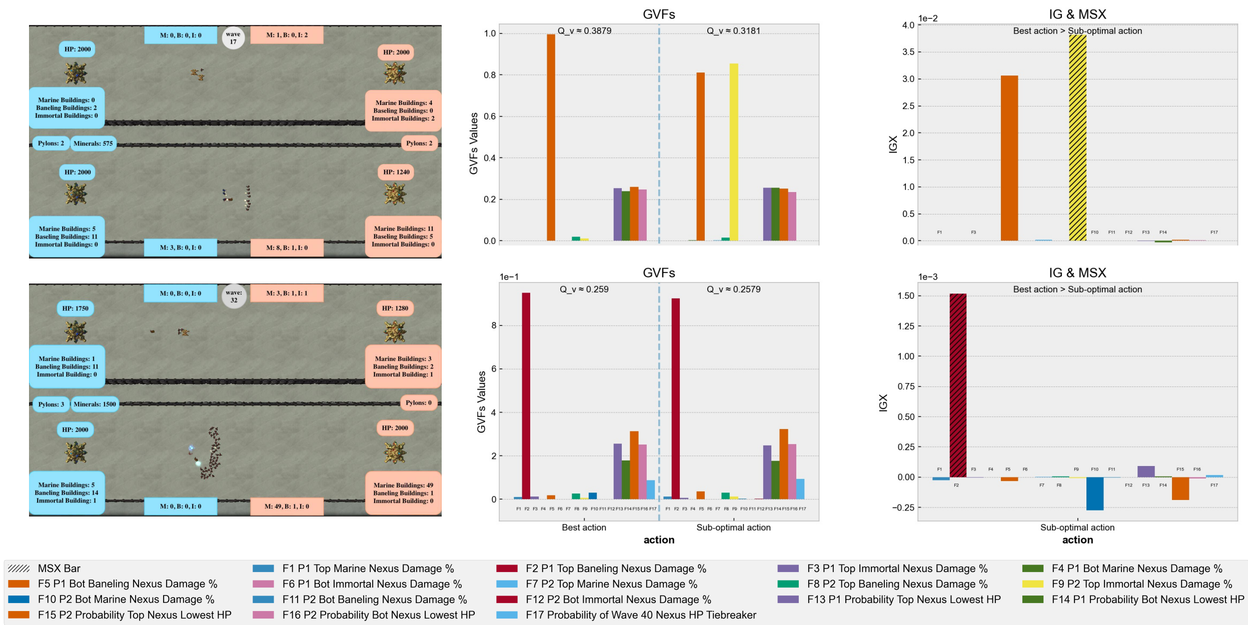

Figure 3: Example Explanations for Tug-of-War 17 feature ESP-DQN agent. Each row shows is for one game state showing: (left) game state; (middle) Q-values and GVFs for preferred action and a non-preferred action; (right) IGX for action pair and corresponding MSX (indicated by highlighted bars). For Game 1 (top) the agent's preferred action is +4 Marine, +1 Baneling in Top Lane and the non-preferred action is +10 Marine, +1 Baneling in Bottom Lane. For Game 2 (bottom) the highest ranked action is +1 Baneling in Bottom Lane and sub-optimal action is +2 Marine, +4 Baneling in Bottom Lane.

most responsible GVF feature for the preference is "damage to the top base from immortals", which agrees with intuition since the best action attempts to defend the top base, while the sub-optimal action does not. Indeed, the GVFs (top) for the sub-optimal action reveals that the top base is predicted to take 80% damage from the enemy's top Immortals in the future compared to nearly 0 for the best action.

In the second game state (bottom), the ESP agent plays against an opponent that it was not trained against and loses by having the bottom base destroyed. The state shows a large enemy attack in the bottom with the ESP agent having enough resources (1500 minerals) to defend if it takes the right action. However, the most preferred action is to add just one Baneling building to the bottom lane, which results in losing. Why was this mistake made?

We compare the preferred action to a lesser-ranked action that adds more buildings to the bottom lane, which should be preferred. The IGX and MSX show (bottom) that the action preference is dominated by the GVF feature related to inflicting damage in the top lane with Banelings. Thus, the agent is "planning" to save minerals to purchase more top lane Baneling buildings in the future. The IGX does indicate that the agent understands that the sub-optimal action will be able to defend the bottom lane better, however, this advantage for the sub-optimal action is overtaken by the optimism about the top lane. This misjudgement of the relative values of these features causes the agent to lose the game. On further analysis, we found that this misjudgement is likely due to the fact that the ESP agent never experienced a loss due to such a bottom lane attack from the opponent it was trained against. This new situation was not properly generalized and suggests training against more diverse opponents.

7. Summary

We introduced the ESP model for producing meaningful and sound contrastive explanations for RL agents. The key idea is to structure the agent's action-value function in terms of meaningful future predictions of its behavior. This allows for action-value differences to be compared in terms of deltas in the future behaviors they entail. To achieve soundness, we ensured that our explanations were formally related to the agent's preferences in a well-defined way. Our case studies provide evidence that ESP models can be learned in non-trivial environments and that the explanations give insights into the agent's preferences. An interesting direction for future work is to continue to enhance the internal structure of the GVFs to allow for explanations at different levels of granularity, which may draw on ideas from GVF networks (11). It is also important to consider user studies to investigate the utility of the approach for identifying agent flaws and improving user's mental models.

References

[1] Akanksha Atrey, Kaleigh Clary, and David Jensen. Exploratory not explanatory: Counterfactual analysis of saliency maps for deep {rl}. In *International Conference on Learning Representations*, 2020.

[2] Samuel Greydanus, Anurag Koul, Jonathan Dodge, and Alan Fern. Visualizing and understanding Atari agents. In Jennifer Dy and Andreas Krause, editors, *Proceedings of the 35th International Conference on Machine Learning*, volume 80 of *Proceedings of Machine Learning Research*, pages 1792–1801, Stockholmsmässan, Stockholm Sweden, 10–15 Jul 2018. PMLR.

[3] Piyush Gupta, Nikaash Puri, Sukriti Verma, Dhruv Kayastha, Shripad Deshmukh, Balaji Krishnamurthy, and Sameer Singh. Explain your move: Understanding agent actions using focused feature saliency. In *International Conference on Learning Representations*, 2020.

[4] Rahul Iyer, Yuezhang Li, Huao Li, Michael Lewis, Ramitha Sundar, and Katia P. Sycara. Transparency and explanation in deep reinforcement learning neural networks. *CoRR*, abs/1809.06061, 2018.

[5] Zoe Juozapaitis, Anurag Koul, Alan Fern, Martin Erwig, and Finale Doshi-Velez. Explainable reinforcement learning via reward decomposition. In *Proceedings of the IJCAI 2019 Workshop on Explainable Artificial Intelligence*, pages 47–53, 2019.

[6] Omar Zia Khan, Pascal Poupart, and James P Black. Minimal sufficient explanations for factored markov decision processes. In *Nineteenth International Conference on Automated Planning and Scheduling*, 2009.

[7] Jelle R Kok and Nikos Vlassis. Sparse cooperative q-learning. In *Proceedings of the twenty-first international conference on Machine learning*, page 61. ACM, 2004.

[8] Volodymyr Mnih, Koray Kavukcuoglu, David Silver, Andrei A Rusu, Joel Veness, Marc G Bellemare, Alex Graves, Martin Riedmiller, Andreas K Fidjeland, Georg Ostrovski, et al. Human-level control through deep reinforcement learning. *Nature*, 518(7540):529–533, 2015.

[9] Matthew L Olson, Lawrence Neal, Fuxin Li, and Weng-Keen Wong. Counterfactual states for atari agents via generative deep learning. *arXiv preprint arXiv:1909.12969*, 2019.

[10] Stuart J Russell and Andrew Zimdars. Q-decomposition for reinforcement learning agents. In *Proceedings of the 20th International Conference on Machine Learning (ICML-03)*, pages 656–663, 2003.

[11] Matthew Schlegel, Adam White, Andrew Patterson, and Martha White. General value function networks. *arXiv preprint arXiv:1807.06763*, 2018.

[12] Mukund Sundararajan, Ankur Taly, and Qiqi Yan. Axiomatic attribution for deep networks. In *Proceedings of the 34th International Conference on Machine Learning-Volume 70*, pages 3319–3328. JMLR. org, 2017.

[13] Richard Sutton, Joseph Modayil, Michael Delp, Thomas Degris, Patrick Pilarski, Adam White, and Doina Precup. Horde : A scalable real-time architecture for learning knowledge from unsupervised sensorimotor interaction categories and subject descriptors. In *International Conference on Autonomous Agents and Multiagent Systems*, volume 2, 2011.

[14] Richard S Sutton and Andrew G Barto. *Reinforcement learning: An introduction*. MIT press, 2018.

[15] Harm Van Seijen, Mehdi Fatemi, Joshua Romoff, Romain Laroche, Tavian Barnes, and Jeffrey Tsang. Hybrid reward architecture for reinforcement learning. In *Advances in Neural Information Processing Systems*, pages 5392–5402, 2017.

[16] Oriol Vinyals, Igor Babuschkin, Junyoung Chung, Michael Mathieu, Max Jaderberg, Wojciech M Czarnecki, Andrew Dudzik, Aja Huang, Petko Georgiev, Richard Powell, et al. Alphastar: Mastering the real-time strategy game starcraft ii. *DeepMind blog*, page 2, 2019.

[17] J Waa, J van Diggelen, K Bosch, and M Neerincx. Contrastive explanations for reinforcement learning in terms of expected consequences. In *Proceedings of the Workshop on Explainable AI on the IJCAI conference, Stockholm, Sweden., 37*, 2018.

[18] Christopher JCH Watkins and Peter Dayan. Q-learning. *Machine learning*, 8(3-4):279–292, 1992.

Supplementary Material
Contrastive Explanations for Reinforcement Learning via Embedded Self Predictions

Zhengxian Lin [1] **Kim-Ho Lam** [1] **Alan Fern** [1]

1. ESP-DQN Pseudo-Code

The Pseudo-code for ESP-DQN is given in Algorithm 1.

2. Convergence Proof for ESP-Table

Algorithm 2 gives the pseudo-code for ESP-Table based on ϵ-greedy exploration. Note that, as for Q-learning, the convergence proof applies to any exploration strategy that guarantees all state-action pairs are visited infinitely often in the limit.

For the proof we will let t index the number of learning updates and $i = \lfloor t/K \rfloor$ be the number of updates to the target tables. The formal statements refer to the *"conditions for the almost surely convergence of standard Q-learing"*. These condition are: 1) There must be an unbounded number of updates for each state-action pair, and 2) The learning rate schedule α_t must satisfy $\sum_t \alpha_t = \infty$ and $\sum_t \alpha_t^2 < \infty$. ESP-Table uses two learning rates, one for the GVF and one for the combining function.

We will view the algorithm as proceeding through a sequence of *target intervals*, indexed by i, with each interval having K updates. We will let $\hat{C}'_i$ and $\hat{Q}'_{F,i}$ denote the target GVF and combining functions, respectively, for target interval i with corresponding target Q-function $\hat{Q}'_i(s,a) = \hat{C}'_i[h(\hat{Q}'_{F,i}[s,a])]$ and greedy policy $\hat{\pi}'_i(s) = \arg\max_a \hat{Q}'(s,a)$. The following lemma relates the targets via the Bellman backup operators. Below for a GVF Q_F we define the max-norm as $|Q_F|_\infty = \max_s \max_a \max_k |Q_{f_k}(s,a)|$.

Lemma 1. *If ESP-Table is run under the standard conditions for the almost surely (a.s.) convergence of Q-learning and uses a Bellman-sufficient pair (F,h) with locally consistent h, then for any $\epsilon > 0$ there exists a finite target update interval K, such that, with probability 1, for all i, $\left|\hat{Q}'_{i+1} - B[\hat{Q}'_i]\right|_\infty \leq \epsilon$ and $\left|\hat{Q}'_{F,i+1} - B_F^{\hat{\pi}'_i}[\hat{Q}'_{F,i}]\right|_\infty \leq \epsilon$.*

That is, after a finite number of learning steps during an interval, the updated target Q-function and GVF are guaranteed to be close to the Bellman backups of the previous target Q-function and GVF. Note that since the targets are arbitrary on the first iteration, these conditions hold for any table-based ESP Q-function.

Proof. Consider an arbitrary iteration i with target functions $\hat{Q}'_i$, $\hat{C}'_i$, $\hat{Q}'_{F,i}$, and let $\hat{Q}^t_i$, $\hat{C}^t_i$, and $\hat{Q}^t_{F,i}$ be the corresponding non-target functions after t updates during the interval. Note that for $t=0$ the non-targets equal to the targets. The primary technical issue is that $\hat{C}^t_i$ is based on a table that can change whenever $\hat{Q}^t_{F,i}$ changes. Thus, the proof strategy is to first show a convergence condition for $\hat{Q}^t_{F,i}$ that implies the table for $\hat{C}^t_i$ will no longer change, which will then lead to the convergence of $\hat{C}^t_i$.

Each update of $\hat{Q}^t_{F,i}$ is based on a fixed target policy $\hat{\pi}'_i$ and a fixed target GVF $\hat{Q}'_{F,i}$ so that the series of updates can be viewed as a stochastic approximation algorithm for estimating the result of a single Bellman GVF backup given by

$$B_F^{\hat{\pi}'_i}[\hat{Q}'_{F,i}](s,a) = F(s,a) + \gamma \sum_{s'} T(s,a,s') \cdot \hat{Q}'_{F,i}[s', \hat{\pi}'_i(s')], \quad (1)$$

which is just the expectation of $F(s,a) + \gamma \hat{Q}'_{F,i}[S', \hat{\pi}'_i(S')]$ with $S' \sim T(s,a,\cdot)$. Given the conditions on the learning rate α_t it is well known that $\hat{Q}^t_{F,i}$ will thus converge almost surely (a.s.) to this expectation, i.e. to $B_F^{\hat{\pi}'_i}[\hat{Q}'_{F,i}]$.[1] The a.s. convergence of $\hat{Q}^t_{F,i}$ implies that for any ϵ' there is a finite t_1 such that for all $t > t_1$, $|\hat{Q}^t_{F,i} - B_F^{\hat{\pi}'_i}[\hat{Q}'_{F,i}]| \leq \epsilon'$. This

[1]Department of EECS, University of Oregon State, Oregon, USA. Correspondence to: Zhengxian Lin <linzhe@oregonstate.edu>, Kim-Ho Lam <lamki@oregonstate.edu>, Alan Fern <Alan.Fern@oregonstate.edu>.

Proceedings of the 37^{th} International Conference on Machine Learning, Vienna, Austria, PMLR 119, 2020.

[1]An "MDP-centric" way of seeing this is to view the update as doing policy evaluation in an MDP with discount factor 0 and stochastic reward function $R(s,a,s') = F(s,a) + \gamma \hat{Q}'_{F,i}(s', \hat{\pi}'_i(s'))$. The convergence of policy evaluation updates then implies our result.

satisfies the second consequence of the lemma if $\epsilon' \leq \epsilon$ and $K > t_1$.

Let $\epsilon' < \epsilon$ be such that it satisfies the local consistency condition of h, which implies that for all $t > t_1$ and all (s, a), $h(\hat{Q}^t_{F,i}[s,a]) = h(B_F^{\hat{\pi}'_i}[\hat{Q}'_{F,i}[s,a])$. That is, after t_1 updates, h will map the non-target GVF to the same table entry as the Bellman GVF Backup of the target GVF and policy. Combining this with the Bellman sufficiency of (F, h) implies that for any state action pairs (s, a) and (x, y), if $h(\hat{Q}^t_{F,i}[s,a]) = h(\hat{Q}^t_{F,i}[x,y])$ then $B[\hat{Q}'_i](s,a) = B[\hat{Q}'_i](x,y)$. This means that after t_1 updates all of the updates to a table entry $h(\hat{Q}^t_{F,i}[s,a])$ have the same expected value $B[\hat{Q}'_i](s,a)$. Using a similar argument as above this implies that $\hat{Q}^t_i(s,a) = h(\hat{Q}^t_{F,i}[s,a])$ converges a.s. to $B[\hat{Q}'_i](s,a)$ for all (s, a) pairs. Let t_2 be the implied finite number of updates after t_1 where the error is within ϵ. The target update interval $K = t_1 + t_2$ satisfies both conditions of the lemma, which completes the proof. □

Using Lemma 1 we can prove the main convergence result.

Theorem 1. *If ESP-Table is run under the standard conditions for the almost surely (a.s.) convergence of Q-learning and uses a Bellman-sufficient pair (F, h) with locally consistent h, then for any $\epsilon > 0$ there exists a finite target update interval K, such that for all s and a, $\hat{\pi}^t(s)$ converges a.s. to $\pi^*(s)$ and $\lim_{t\to\infty} |\hat{Q}^t_F(s,a) - Q^{\pi^*}_F(s,a)| \leq \epsilon$ with probability 1.*

Proof. From Lemma 1 we can view ESP-Table as performing approximate Q-value iteration, with respect to the sequence of target functions $\hat{Q}'_i$. That is, the total updates done during a target interval define an approximate Bellman backup operator $\hat{B}$, such that $\hat{Q}'_{i+1} = \hat{B}[\hat{Q}'_i]$. Specifically, there exists a K, such that the approximate operator is ϵ-accurate, in the sense that for any Q-function Q, $\left|\hat{B}[Q] - B[Q]\right|_\infty \leq \epsilon$.

Let $\hat{B}^i[Q]$ denote i applications of the operator starting at Q so that $\hat{\pi}'_i$ is the greedy policy with respect to $\hat{B}^i[\hat{Q}'_0]$. Prior work (1) implies that for any starting Q, the sub-optimality of this greedy policy is bounded in the limit.

$$\limsup_{i\to\infty} \left|V^* - V^{\hat{\pi}'_i}\right|_\infty \leq \frac{2\beta}{(1-\beta)^2}\epsilon \tag{2}$$

where V^* is the optimal value function and V^π is the value function of a policy π.

Now let

$$\delta = \min_\pi \min_{s: V^*(s) \neq V^\pi(s)} |V^*(s) - V^\pi(s)|$$

be smallest non-zero difference between an optimal value at a state and sub-optimal value of a state across all non-optimal policies. From this definition it follows that, if $\left|V^* - V^{\hat{\pi}^i}\right|_\infty \leq \delta$, then $\hat{\pi}^i = \pi^*$. From Equation 2 this condition is achieved in the limit as $i \to \infty$ if we select $\epsilon < \frac{(1-\beta)^2}{2\beta}\delta$. Let K_1 be the finite target interval implied by Lemma 1 to achieve this constraint on ϵ. Since Lemma 1 holds with probability 1, we have proven that $\hat{\pi}'_i$ converges almost surely to π^* for a finite K_1. This implies the first part of the theorem.

For the second part of the theorem, similar to the above reasoning, Lemma 1 says that we can view the target GVF $\hat{Q}'_{F,i}$ as being updated by an approximate Bellman GVF operator $\hat{B}_F^{\hat{\pi}'_i}$. That is, for any GVF Q_F and policy π, $\left|B^\pi_F[Q_F] - \hat{B}^\pi_F[Q_F]\right|_\infty \leq \epsilon$. Further, it is straightforward to show that our approximate Bellman GVF operator satisfies an analogous condition to Equation 2, but for GVF evaluation accuracy in the limit. In particular, for any π and initial Q_F, if we define $\hat{Q}^\pi_{F,i}$ to be the GVF that results after i approximate backups the following holds.[2]

$$\limsup_{i\to\infty} \left|Q^\pi_F - \hat{Q}^\pi_{F,i}\right|_\infty \leq \frac{\epsilon}{(1-\gamma)}. \tag{3}$$

Thus, for a fixed policy the approximate backup can be made arbitrarily accurate for small enough ϵ.

From the almost sure convergence of $\hat{\pi}'_i$, we can infer that there exists a finite i^* such that for all $i > i^*$, $\hat{\pi}'_i = \pi^*$. Thus, if $K > K_1$, then after the i^* target update the target policy will be optimal thereafter. At this point the algorithm enters a pure policy evaluation mode for fixed policy π^*, which means that the approximate GVF operator is continually being applied to π^* across target intervals. From Equation 3 this means that in the limit as $i \to \infty$ we have that

$$\limsup_{i\to\infty} \left|Q^{\pi^*}_F - \hat{Q}'_{F,i}\right|_\infty \leq \frac{\epsilon}{(1-\gamma)}.$$

Thus, we can achieve any desired accuracy tolerance in the limit by selecting a small enough ϵ. Let K_2 be the target interval size implied by Lemma 1 for that epsilon and let the target interval be $K = \max\{K_1, K_2\}$. This implies that using a target interval K, there is a finite number of target updates i' after the first i^* updates such that for all $i > i^* + i'$, $\hat{Q}'_{F,i}$ will achieve the error tolerance. This completes the second part of the proof. □

[2]This can be proved via induction on the number of exact and approximate Bellman GVF backups, showing that after i backups the difference is at most $\epsilon \sum_{j=0}^{i-1} \gamma^j$ and then taking the limit as $i \to \infty$.

3. Tug of War Domain

In this section, we overview the real-time strategy (RTS) game, 'Tug of War' (ToW), used for this study. Tug of War (ToW) is an adversarial two-player zero-sum strategy game we designed using Blizzard's PySC2 interface to Starcraft 2. Tug of War is played on a rectangular map divided horizontally into top and bottom lanes as shown in Figure 1. The game is viewed from an omnipotent camera position looking down at the map. Each lane has two base structures; Player 1 owns the two bases on the left of the map, and Player 2 owns the two bases on the right. The game proceeds in 30 second waves. Before the next wave begins, players may select either the top or bottom lane for which to purchase some number of military-unit production buildings with their available currency.

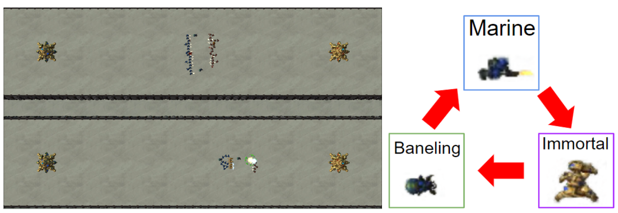

Figure 1: (left) Tug of War game map - Top lane and bottom lane, Player 1 owns the two bases on the left (gold star-shaped buildings), Player 2 owns the two bases on the right. Troops from opposing players automatically march towards their opponent's side of the map and attack the closest enemy in their lane. (right) Unit Rock Paper Scissors - Marines beats Immortals, Immortals beats Banelings, and Banelings beats Marines. We have adjusted unit stats in our custom Starcraft 2 map to befit ToW's balance.

We have designed Tug of War allowing AI vs AI, Human vs Human, and AI vs Human gameplay. Watch a Human vs Human ToW game from Player 1's perspective here: https://peertube.live/videos/watch/2cada211-2ebc-49a5-817b-5217088fc832

Each purchased building produces one unit of the specified type at the beginning of each wave. Buildings have different costs and will require players to budget their capital. These three unit types, Marines, Immortals, and Banelings, have strengths and weaknesses that form a rock-paper-scissors relationship as shown in Figure 1. Units automatically move across the lanes toward the opponent's side, engage enemy units, and attack the enemy base if close enough. Units will only attack enemy troops and bases in their lane. If no base is destroyed after 40 waves, the player who owns the base with the lowest health loses.

Both Players receive a small amount of currency at the beginning of each wave. A player can linearly increase this stipend by saving to purchase up to three expensive economic buildings, referred to as a Pylon.

ToW is a near full-information game; players can see the all units and buildings up to the current wave. Both player's last purchased buildings are revealed the moment after a wave spawns. The only hidden information is the unspent currency the opponent has saved; one could deduce this value as the wave number, cost of each building, currency earned per wave, and the quantities of buildings up to the current snapshot are known. It would be difficult for a human to perform this calculation quickly.

Tug of War is a stochastic domain where there is slight randomness in how opposing units fight and significant uncertainty to how the opponent will play. Winning requires players assessing the current state of the game and balancing their economic investment between producing units immediately or saving for the future. Players must always be mindful of what their opponent may do so as to not fall behind economically or in unit production. Purchasing a Pylon will increase one's currency income and gradually allow the player to purchase more buildings, but players must be wary as Pylons are expensive, saving currency means not purchasing unit-production buildings which may lead to a vulnerable position.Conversely, if the opponent seems to be saving their currency, the player can only guess as to what their opponent is saving for; the opponent may be saving to purchase a Pylon or they may be planning to purchase a lot of units in a single lane.

Tug of War presents a challenging domain to solve with Reinforcement Learning (RL). These challenges include a large state space, large action space, and sparse reward. States in ToW can have conceivably infinite combinations of units on the field, different quantities of buildings in lanes, or different base health. The number of possible actions in a state corresponds to the number of ways to allocate the current budget, which can range from 10s to 1000s. Finally, the reward is sparse giving +1 (winning) or 0 (losing) at the end of the game, where games can last up to 40 waves/decisions.

3.1. Tug of War Feature Design

While humans need continuous visual feedback to interact with video games, computer systems can use simple numeric values received in disjointed intervals to interpret game state changes. We have designed an abstract "snapshot" of the ToW game state at a single point in time represented as a 68 dimensional feature vector. Note that for this study, we have increased added additional features to capture granular details, thus bringing the total to 131 features. At the last moment before a wave spawns, the AI agent receives this feature snapshot and uses it to select an action for the next wave. We call this moment a decision point. The decision point is the only time when the agent receives information about the game and executes an action; the agent does not continuously sample observations from the game. The agent's performance indicates this abstraction is sufficient for it to learn and play the game competently.

The state feature vector includes information such as the current wave number, health of all 4 bases, the agent's current unspent currency, the agent's current building counts in both top and bottom lanes, the enemy's last observed building counts in the top and bottom lanes, pylon quantities, and the number of troops in each grid of the 4 grid sections of the map as depicted in Figure 2. opponent's current unspent mineral count is not sent to the agent as this hidden information is part of the game's design.

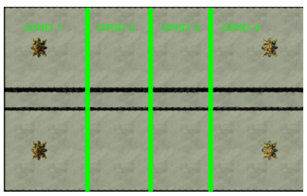

Figure 2: ToW 2 Lane 4 Grid - Unit quantities and positions on the map is descretized into four sections per lane.

4. Agent Details: Hyperparameters and Architectures

The ESP agent code is provided in Supplementary Material, including pre-trained models for all domains we present.

Table 1 gives the hyperparameters used in our implementation. Note that our implementation of ESP-DQN supports both hard target updates as shown in the pseudo-code and "soft target updates" (2), where at each step the target network parameters are gradually moved toward the currently learned parameters via a mixing proportion τ. We found that this can sometimes lead to more stable learning and use it in two of our domains as indicated in the table.

Table 2 presents our GVF network structures used to train the agents in each domain We use identity activations for the GVF outputs. We use Sigmoid functions on F1 through F12 and F17 features for our Tug of War ESP-DQN 17-feature agent and on F131 for our Tug of War ESP-DQN 131-feature agent because the data ranges $(0, 1)$. We apply a SoftMax function to features F13 to F16 and F1 to F8 for our our Tug of War ESP-DQN 17-feature and 131-feature agents because said features correspond to probabilities that sum to 1.

5. Tug of War 131 Features

We introduce a detailed description of the 131 features used to train our Tug of War ESP-DQN agent. These features capture events in ToW, namely:

- Game ending win-condition probabilities; The likelyhood for each base to be destroyed or have the lowest HP at wave 40.
- P1 and P2 currency; These features allow GVFs to predict the amount of money players will receive in the future.
- Quantity of units spawned.
- The number of each type of units will be survive at different ranges [4] we defined on the map for both players; allowing the GVFs to predict the advantage of each lane of each type of unit in the future.
- Delta damage to each of the four bases by each of the three unit types. These features allow GVFs to predict the amount of damage each unit type will inflict on the opponent's base in the unit's respective lane.
- The amount of damage inflicted by which type of units on another type of units for both players, like the damage the friendly Marine inflicted on enemy immortal; Allows the GVFs to predict the amount damage for each type of units inflicting on each type of units.
- An indicator of whether the game reaches waves of tie-breaker.

6. Example Explanations

Lunar Lander. Figure 3(a) shows a state in Lunar Lander entered by a near-optimal learned ESP policy. The state is dangerous due to the fast downward and clockwise rotational velocity depicted by the arrows. Figure 3(b) shows the Q-values for the actions and the predicted GVF bars. We see that the "main engine" and "right engine" actions have nearly the same Q-values with "main engine" slightly preferred, while "left engine" and "noop" are considered significantly worse. We would like to understand and assess the rationale for the strong preferences and the weak preferences.

While a user can observe differences among GVFs across actions, it is not clear how they relate to the overall preferences. Figure 3(c) shows the IGXs corresponding to the preference of "main engine" over the other three actions. In addition, the MSX is depicted via dashed lines over IGX components in the MSX (usually only a single component). Focusing first on the larger preferences, we see that "main

[4]In addition to the 4 grid map regions as explained in Figure 2, we add a 5th map region (Grid 5) to detect units attacking bases. Grid 5 for P1 is indicates the quantity of P1 units attacking P2's bases. This is reversed for P2, where now Grid 1 for P2 indicates P2 units attacking P1's bases.

Hyper-Parameters	Lunar Lander	Cart Pole	Tug-of-War(both)
Discount factors(γ and β)	0.99	0.99	0.9999
Learning Rate(α)	10^{-4}	10^{-5}	10^{-4}
Start Exploration(ϵ_s)	1.0	1.0	1.0
Final Exploration(ϵ_f)	0.01	0.05	0.1
Exploration Decrease(linearly) Steps	$2 * 10^5$	$2 * 10^5$	$4 * 10^4$
Batch Size	128	128	32
Soft/Hard Replace	Soft	Soft	Hard
Soft Replace(τ)	$5 * 10^{-4}$	$5 * 10^{-4}$	N/A
Hard Replace Steps	N/A	N/A	$6 * 10^3$
GVF Net Optimizer	Adam	Adam	Adam
Combiner Net Optimizer	SGD	SGD	SGD
Training Episodes	$5 * 10^3$	10^4	$1.3 * 10^4$
Evaluation Intervals	200	100	40
Evaluation Episodes	100	100	10
Riemann approximation steps of IGX[3]	30	30	30

Table 1: Hyper-parameters and optimizers used to train our ESP-DQN and DQN agents on Lunar Lander, Cart Pole and Tug of War.

	Lunar Lander	Cart Pole	Tug-of-War(17f)	Tug-of-War(131f)
GVF Net	3 layers MLP	3 layers MLP	4 layers MLP	4 layers MLP
Functions on GVF outputs	None	None	Sigmoid(F1-F12, F17) SoftMax(F13-F16)	SoftMax(F1-F8) Sigmoid(F131)
Combiner Net	3 layers MLP	3 layers MLP	4 layers MLP	4 layers MLP

Table 2: Network structures we used to train our ESP-DQN and DQN agents on Lunar Lander, Cart Pole and Tug of War.

engine” is preferred to “left engine” primarily due to GVF differences in the velocity and landing features, with the MSX showing that landing alone is sufficient for the preference. This rationale agrees with common sense, since the left engine will accelerate the already dangerous clockwise rotation requiring more extreme actions that put the future reward related to landing at risk.

For the preference over “noop” the velocity feature dominates the IGX and is the only MSX feature. This agrees with intuition since by doing nothing the dangerous downward velocity will not be addressed, which means the landing velocity will have a more negative impact on reward. Comparing “main engine” to the nearly equally valued “right engine” shows that the slight preference is based on the distance and right leg landing feature. This is more arbitrary, but agrees with intuition since the right engine will both reduce the downward velocity and straighten the ship, but will increase the leftward velocity compared to the main engine. This puts it at greater risk of reducing reward for missing the right leg landing goal and distance reward. Overall the explanations agreed well with intuition, which together with similar confirmation can increase our confidence in the general reasoning of the policy. We also see the MSXs were uniformly very small.

Figure 3(d) illustrates another Lunar Lander state achieved by a near-optimal ESP policy. The lander is moving down to the left and is close to landing within the goal. Additionally, the left leg has touched the ground as marked by the green dot. Figure 3(e) shows the GVF values of all actions and expects the lander to land successfully with the right leg touching down. The GVFs values of the distance, velocity, and angle are small because the lander is close to the goal.

Although this state allows the lander to successfully land after taking any action, the IGX shown in Figure 3(f) illustrates the agent prefers “use left engine”. This is because using the right engine will increase the velocity of the lander, pushing it towards the left and increasing “F1 Distance” from the goal. This action and justification makes intuitive sense as the lander is unlikely to fail in this state and has chosen an action that reduces its velocity and decreases its landing delay.

The “use main engine” action also delays the landing increases distance to the goal, as indicated by the MSX bars in Figure 3(f). The IGX also shows the “use main engine” engine risks the left leg leaving the ground which agrees with intuition as moving up pushes the lander back into space. However, “use main engine” gives the lander another opportunity to adjust its velocity and angle. That may be

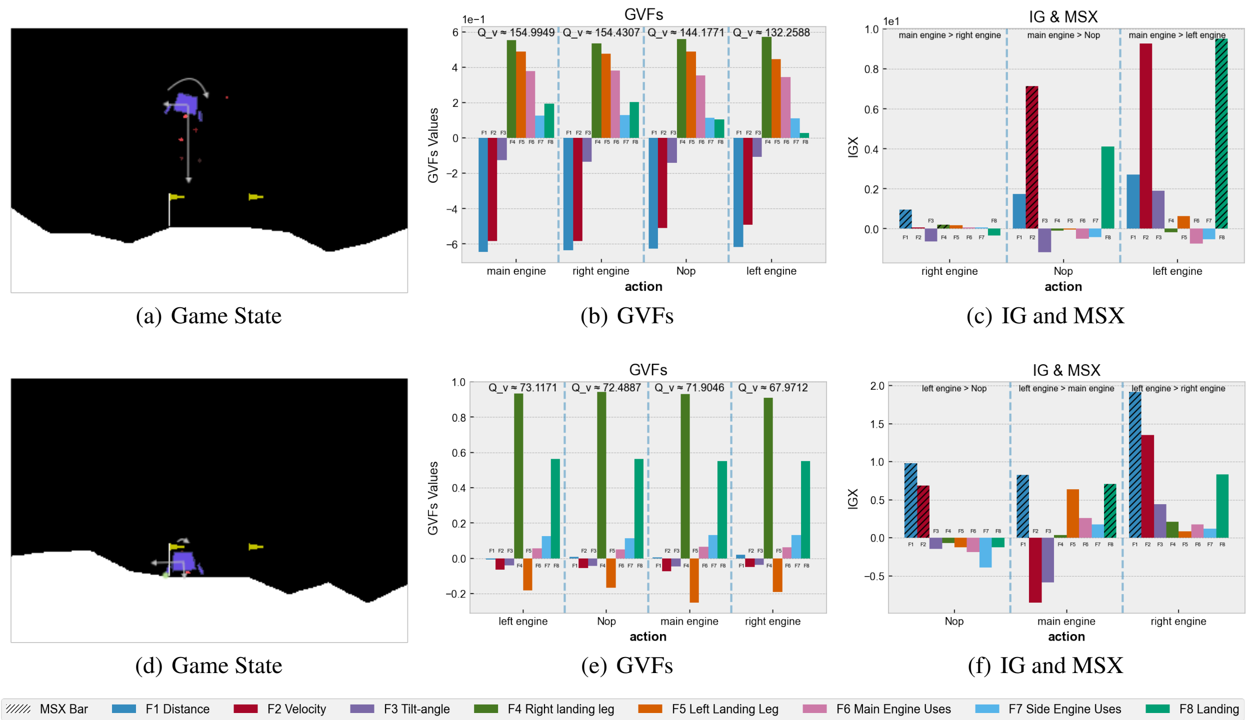

(a) Game State (b) GVFs (c) IG and MSX

(d) Game State (e) GVFs (f) IG and MSX

Figure 3: Two explanation examples for Lunar Lander. Each row shows the game state, the Q-values and GVF predictions for actions, and the IGX and MSX respectively.

why the IGX of velocity and tile-angle are negative. The "no-op" action has a lower preference than the best action because the lander is slightly drifting and may move out of the goal. Two largest IGXs of "noop" action agrees with this rationale. However, the IGX of landing is negative that may be arbitrary or indicates doing the "noop" action will lead the lander to land faster since the lander is moving down already, but sometimes landing faster gets less reward because moving to the center of the goal can gain more reward by reducing the distance between the center of goal and lander.

Cart Pole. Figure 4(a) shows a Cart Pole state encountered by a learned near-optimal ESP policy, where the cart and the pole are moving in the left direction with the pole angle being in a dangerous range already. The action "push left" is preferred over "push right", which agrees with intuition. We still wish to verify that the reasons for the preference agree with our common sense. From the IGX and MSX in Figure 4(c) the primary reason for the preference is the "pole angle left" GVF, which indicates that pushing to the right will lead to a future where the pole angle spends more time in the dangerous left region. Interestingly we see that "push right" is considered advantageous compared to "push left" with respect to the left boundary and left velocity features, which indicates some risk for push left with respect to these components. All of these preference reasons agree with intuition and along with similar examples can build our confidence in the agent.

Tug of War: 17 Features. Figure 5(a) depicts a screenshot of a Tug of War (ToW) game where our ESP agent (P1, blue) is playing against a new AI opponent (P2, orange) it has never encountered. The ESP agent's top base is destroyed after two waves thus losing the game. The annotated game state shows the ESP agent doesn't have enough units to defend its top base as its opponent's banelings can kill almost all its units, and the agent's Top lane base has approximately 35% hit points (HP) remaining. We can regard this state as a critical moment in the game because the agent spends all its money to defend the top lane and still looses the base in two waves after taking the its highest ranked action. Given our deep ToW game knowledge, we want to understand why the ESP agent chose to purchase Banelings in the Bottom Lane (arguably sub-optimal) rather than purchase Immortals in the Top Lane (intuitively a better action).

To understand why the agent prefers the action that is worse than an action we intuitively recognize to be better, we analyze both action's GVFs (Figure 5(b)), and IG & MSX (Figure 5(c)). The sub-optimal action's GVFs shows the sub-optimal action is expected to reduce damage from the enemy's top Banelings. This indicates the agent understands taking the sub-optimal action can pose a better defense. However, the MSX bar shows positive IGX of the self bottom Baneling damage still can cover the negative IGX of enemy top Baneling damage; indicating the agent is focusing on destroying the enemy's bottom base while ig-

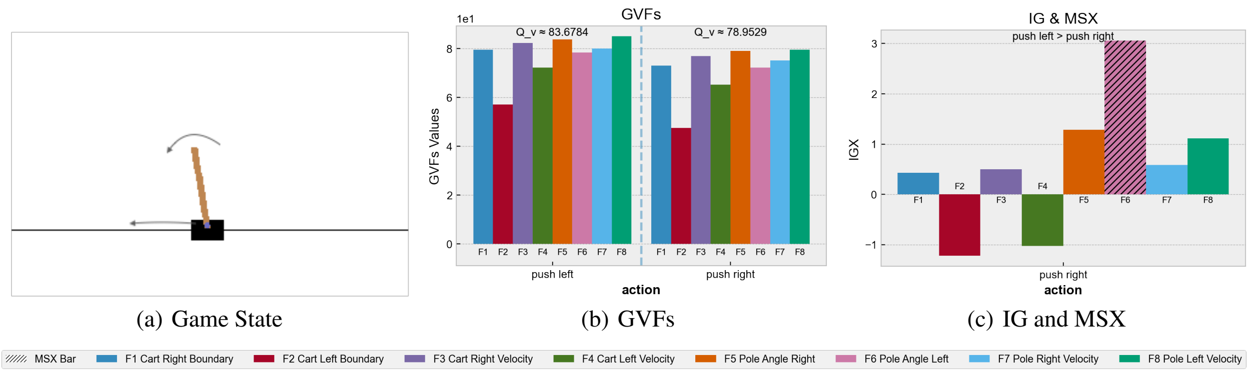

(a) Game State (b) GVFs (c) IG and MSX

Figure 4: Explanation example for Cart Pole. Three Figures show the game state, the Q-values and GVF predictions for actions, and the IGX and MSX respectively.

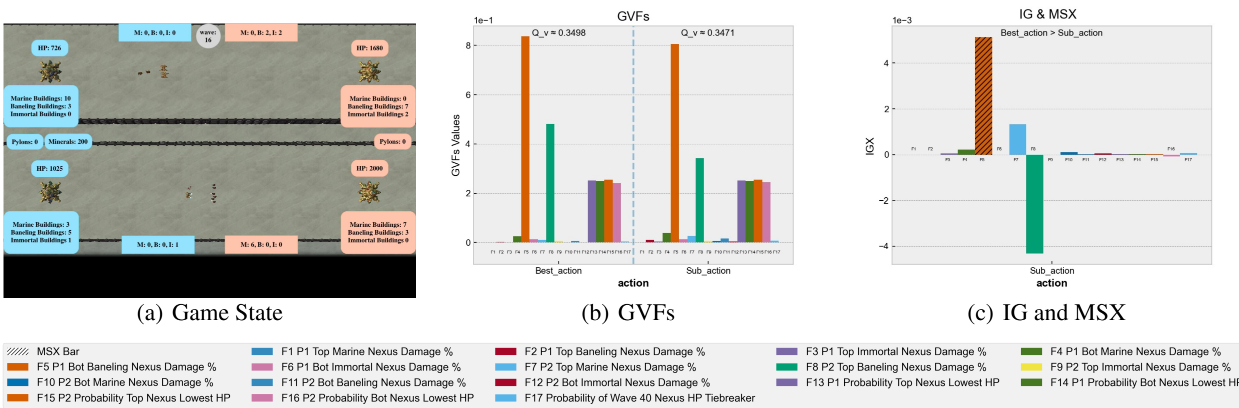

(a) Game State (b) GVFs (c) IG and MSX

Figure 5: Explanation example for Tug-of-War 17 feature ESP-DQN agent. Three Figures show the game state, the Q-values and GVF predictions for actions, and the IGX and MSX respectively. The top ranked action +2 Baneling in Bottom Lane and sub-optimal is +1 Immortals in Top Lane.

noring the damage its top base will take. This misjudgement can be attributed to the agent over-fitting to its fixed-agent opponent during training.

Tug of War: 131 Features. Figure 5(a) depicts a screenshot of a Tug of War game where our (P1, blue) ESP agent is playing against the same fixed-policy AI opponent (P2, orange) it was trained against. The ESP agent wins by destroying the opponent's bottom base. The state in Figure 6(a) indicates both players have a balanced quantity of units in the top lane. We also observe P2 has an advantage in the bottom lane as the ESP agent doesn't have enough units to defend. The ESP agent has determined its best action is to spend all its money on producing +8 Marine buildings in the Bottom Lane to defend, which agrees with intuition as Marines counter Immortals. To justify why one can regard this choice as optimal, we compare the agent's best-determined action, +8 Marine buildings in Bottom Lane, to a sub-optimally ranked action, +5 Baneling buildings in Bottom Lane, due to Immortals counter Banelings.

Figure 6(b) shows the GVF value of both action. Given the dense nature of the 131 Features, we summarize the following:

- The values concerning accumulated quantity features such as future currency to be earned are higher in the sub-optimal action than the best action because the game is expected to be prolonged if a sub-optimal action is taken. The probability to end the game by tie-breaker(F131) as shown in Figure 6(b), graph "Probability to End by Tie-breaker" agrees taking the best action leads to a faster win.
- The sub-optimal action raises the probability of our ESP agent's bottom base getting destroyed(F2) and lowers the probability of the opponent's bottom base getting destroyed(F4). This assessment agrees with the game rules as Banelings do little to counter Immortals.
- Agent's Expected Bottom Marine to Spawn(F14) is higher of if it takes the best action, and Expected Bottom Baneling to Spawn(F15) is higher if takes sub-optimal action.

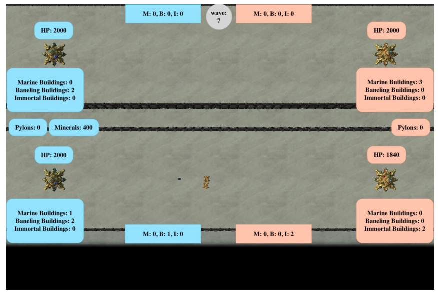

(a) Game State

(b) GVFs

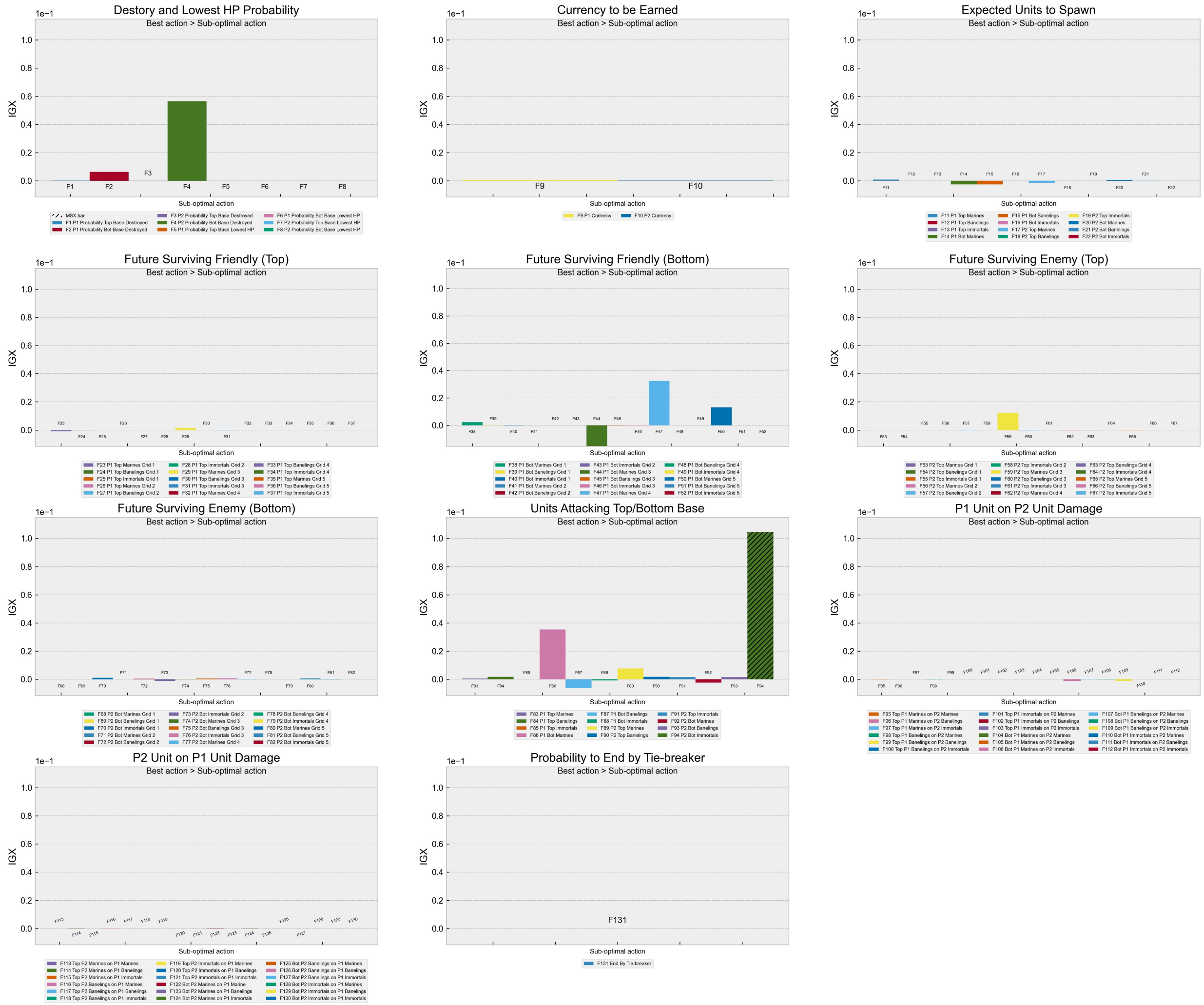

(c) IG and MSX

Figure 5: Explanation example for Tug-of-War 131 feature ESP-DQN agent. Since there are too much features to show as one figure, we separate them into 11 clusters. Three Figures show the game state, the Q-values and GVF predictions for actions, and the IGX and MSX respectively. The top ranked action +8 Marines in Bottom Lane and sub-optimal is +5 Banelings in Bottom Lane.

- By taken the best action, the agent expects its future surviving bottom marines to be closer to P2's bottom base(F44, F47 and F50); indicating the agent's units are able to push the enemy back. Contrasted to the sub-optimal action, where the opponent's surviving bottom Immortal is expected to be closer to the ESP agent's bottom base(F70, F73 and F76), indicating the opponent pushed the agent back.

- If the ESP agent purchases +8 marines in the bottom lane (best ranked action), the agent expects to take no damage from the enemy(F89 to F94). This can be contrasted to the expected damage if the agent were to purchase +5 baneling buildings in the bottom lane (sub-optimal action) where the agent expects to take base damage from P2's immortals(F94) as shown in Figure 6(b), graph "Units Attacking Top/Bottom Base".

- We can validate the agent understands the rock-paper-scissor interaction between marines, banelings, and immortals from the GVF graphs as shown in Figure 6(b), graph "P1 Unit on P2 Damage" and "P2 Unit on P1 Damage". If the agent produces marines, the ESP agent correctly expects to inflict a large amount of damage on P2's immortals. If the agent produces banelings, the ESP agent correctly expects to inflict a large amount of damage on P2's marines.

- There exist some flaws in the agent's GVF predictions. Some values such as Future Surviving Units in Figure 6(b) should not be negative, indicating some flaw in the agent's training. This suggests an engineer can add a ReLU function on the output to prevent negative values.

Explanations produced by our ESP model are sound because said explanations do not depend on GVF comparisons alone. Figure 6(c), graph "Units Attacking Top/Bottom Base" illustrates P2 Immortal Damage on bottom base (F94); the primary MSX contribution for why the agent ranked +8 marine buildings as its best action. Given the notion that P2's Immortals in the bottom lane presents a significant threat, producing marines to defend the immortals makes good intuitive sense. Banelings are a sub-optimal choice in this scenario, and would do little to defend against Immortals. We summarize the IG and MSX graph in Figure 6(c) as follows,

- The best action adds more Marine buildings; thus increasing the quantity of marines spawned per wave, but the agent doesn't care about the quantity of marines(F14) as the IGX is close to 0. However, the agent cares about the damage the Marine inflict (F86), although this is not as important as defending against opponent's Immortals.

- Graph "Destroy and Lowest HP Probability" illustrates the two mutually exclusive win types in ToW; winning by destroying one of P2's bases, or winning by making sure one of P2's base has the lowest HP at wave 40. The probability Base Destroyed IGX indicates the agent expects to destroy the opponent's bottom base(F4) and defend its own bottom base(F2).

- Graph "Future Surviving Friendly (Bottom)" illustrates the contribution of P1's surviving troops in the bottom lane. The positive IGX contribution of feature "P1 Bottom Marine Grid 4(F47)" and "Grid 5(F50)" indicates the agent cares about its marines moving closer to the enemy's bottom base. The IGX of the "P1 Bot Marine Grid 3(F44)" is negative, possibly because Grid 3 is too far from the opponent's base to be considered a disadvantage.

Given the large number of features, the MSX is critical to get a quick understanding of the agent's preference. In general, user interface design will be an important consideration when the number of features is large. Such interfaces should allow users to incrementally explore the IGX and GVFs of different actions flexibly and on demand.

References

[1] Dimitri P Bertsekas and John N Tsitsiklis. *Neuro-dynamic programming*. Athena Scientific, 1996.

[2] Timothy P Lillicrap, Jonathan J Hunt, Alexander Pritzel, Nicolas Heess, Tom Erez, Yuval Tassa, David Silver, and Daan Wierstra. Continuous control with deep reinforcement learning. *arXiv preprint arXiv:1509.02971*, 2015.

[3] Mukund Sundararajan, Ankur Taly, and Qiqi Yan. Axiomatic attribution for deep networks. In *Proceedings of the 34th International Conference on Machine Learning-Volume 70*, pages 3319–3328. JMLR. org, 2017.

Algorithm 1 ESP-DQN: Pseudo-code for ESP-DQN agent Learning.

Require: Act(s, a) ;; returns tuple $(s', r, F, done)$ of next state s', reward r, GVF features $F \in R^n$, and terminal state indicator $done$
Require: K - target update interval, β - reward discount factor, γ - GVF discount factor
  Init $\hat{Q}_F$, $\hat{Q}'_F$;; The non-target and target GVF networks with parameters θ_F and θ'_F respectively.
  Init $\hat{C}$, $\hat{C}'$;; The non-target and target combining networks with θ_C and θ'_C rspectively.
  Init $M \leftarrow \emptyset$;; initialize replay buffer
  ;; Q-function is defined by $\hat{Q}(s, a) = \hat{C}(\hat{Q}_F(s, a))$
  ;; Target Q-function is defined by $\hat{Q}'(s, a) = \hat{C}'(\hat{Q}'_F(s, a))$
  repeat
    Environment Reset $s_0 \leftarrow$ Initial State totalUpdates $\leftarrow 0$
    for $t \leftarrow 0$ to T **do**
      $a_t \leftarrow \epsilon(\hat{Q}, s_t)$ // ϵ-greedy
      $(s_{t+1}, r_t, F_t, done_t) \leftarrow$ Act(s_t, a_t)
      Add $(s_t, a_t, r_t, F_t, s_{t+1}, done_t)$ to M

      ;; update networks
      Randomly sample a mini-batch $\{(s_i, a_i, r_i, F_i, s'_i, done_i)\}$ from M
      $\hat{a}_i \leftarrow \arg\max_{a \in A} \hat{Q}'(s'_i, a)$
      $f'_i \leftarrow \begin{cases} F_i & \text{If } done_i \text{ is} \\ F_i + \gamma \hat{Q}'_F(s'_i, \hat{a}_i) & \text{Otherwise} \end{cases}$
      $q'_i \leftarrow \begin{cases} r_i & \text{If } done_i \text{ is} \\ r_i + \beta \hat{Q}'(s'_i, \hat{a}_i) & \text{Otherwise} \end{cases}$
      Update θ_F via gradient descent on average mini-batch loss $(f'_i - \hat{Q}_F(s_i, a_i))^2$
      Update θ_C via gradient descent on average mini-batch loss $(q'_i - \hat{Q}(s_i, a_i))^2$

      if totalUpdates mod $K == 0$ **then**
        $\theta'_F \leftarrow \theta_F$
        $\theta'_C \leftarrow \theta_C$
      end if
      totalUpdates $\leftarrow$ totalUpdates $+ 1$

      if $done_t$ is **then**
        break
      end if
    end for
  until convergence

Algorithm 2 ESP-Table: Pseudo-code for a table-based variant of ESP-DQN. The notation $Q \xleftarrow{\alpha} x$ is shorthand for $Q \leftarrow (1 - \alpha)Q + \alpha x$.

Require: Act(s, a) ;; returns tuple (s', r, F) of next state s', reward r, and GVF features $F \in R^n$
Require: $h(q)$ - hash function from R^n to a finite set of indices I
Require: K - target update interval
Require: γ, β - discount factors for GVF and reward respectively
  Init $\alpha_{F,0}$, $\alpha_{F,0}$;; learning rates for GVF and combining function
  Init $\hat{Q}_F[s, a]$;; GVF table indexed by state-action pairs
  Init $\hat{C}[i]$;; Combining function table indexed by indices in I
  Init $\hat{Q}'_F[s, a]$;; Target GVF table indexed by state-action pairs
  Init $\hat{C}'[i]$;; Target Combining function table indexed by indices in I
  ;; Q-function is defined by $\hat{Q}(s, a) = \hat{C}[h(\hat{Q}_F[s, a])]$
  ;; Target Q-function is defined by $\hat{Q}'(s, a) = \hat{C}'[h(\hat{Q}'_F[s, a])]$

  $s_0 \leftarrow$ Initial State
  $t = 0$
  repeat
    if t mod $K == 0$ **then**
      $\hat{Q}'_F \leftarrow \hat{Q}_F$
      $\hat{C}' \leftarrow \hat{C}$
    end if
    $a_t \leftarrow \epsilon(\hat{Q}, s_t)$;; ϵ-greedy exploration
    $(s_{t+1}, r_t, F_t) \leftarrow$ Act(s_t, a_t)
    $a' \leftarrow \arg\max_a \hat{Q}'(s_{t+1}, a)$
    $\hat{Q}_F[s_t, a_t] \xleftarrow{\alpha_{F,t}} F_t + \gamma \hat{Q}'_F(s_{t+1}, a')$
    $\hat{C}[h(\hat{Q}_F[s_t, a_t])] \xleftarrow{\alpha_{C,t}} r_t + \beta \hat{Q}'(s_{t+1}, a')$
    $t \leftarrow t + 1$
  until convergence